Published in final edited form as:
J Synchrotron Radiat. 2001 March 1; 8(0 2): 199–203.

High-resolution X-ray spectroscopy of rare events: a different look at local structure and chemistry

Uwe Bergmann[a,b], **Pieter Glatzel**[b], **John H. Robblee**[a], **Johannes Messinger**[a], **Carmen Fernandez**[a], **Roehl Cinco**[a], **Henk Visser**[a], **Karen McFarlane**[a], **Emanuele Bellacchio**[a], **Shelly Pizarro**[a], **Kenneth Sauer**[a], **Vittal K. Yachandra**[a], **Melvin P. Klein**[a], **Billie L. Cox**[c], **Kenneth H. Nealson**[c], and **Stephen P. Cramer**[a,b]

Uwe Bergmann: u_bergmann@lbl.gov

[a]Physical Biosciences Division, Lawrence Berkeley National Laboratory, Berkeley, CA 94720, USA

[b]Department of Applied Science, University of California, Davis, CA 95616, USA

[c]CALTECH, Jet Prop Lab, 183-301, 4800 Oak Grove Dr Pasadena, CA 91109, USA

Abstract

The combination of large-acceptance high-resolution X-ray optics with bright synchrotron sources permits quantitative analysis of rare events such as X-ray fluorescence from very dilute systems, weak fluorescence transitions or X-ray Raman scattering. Transition-metal $K\beta$ fluorescence contains information about spin and oxidation state; examples of the characterization of the Mn oxidation states in the oxygen-evolving complex of photosystem II and Mn-consuming spores from the marine bacillus SG-1 are presented. Weaker features of the $K\beta$ spectrum resulting from valence-level and ‘interatomic’ ligand to metal transitions contain detailed information on the ligand-atom type, distance and orientation. Applications of this spectral region to characterize the local structure of model compounds are presented. X-ray Raman scattering (XRS) is an extremely rare event, but also represents a unique technique to obtain bulk-sensitive low-energy (<600 eV) X-ray absorption fine structure (XAFS) spectra using hard (~10 keV) X-rays. A photon is inelastically scattered, losing part of its energy to promote an electron into an unoccupied level. In many cases, the cross section is proportional to that of the corresponding absorption process yielding the same X-ray absorption near-edge structure (XANES) and extended X-ray absorption fine structure (EXAFS) features. XRS finds application for systems that defy XAFS analysis at low energies, *e.g.* liquids or highly concentrated complex systems, reactive compounds and samples under extreme conditions (pressure, temperature). Recent results are discussed.

Keywords

X-ray fluorescence spectroscopy; X-ray Raman scattering; inelastic scattering; high resolution; metalloproteins

Correspondence to: Uwe Bergmann, u_bergmann@lbl.gov.

1. Introduction

The interaction of X-rays with matter forms the basis for many techniques to study local structure and chemistry of condensed matter. In this paper, some less established cases are presented, all concerning rare events. Two examples with quite different origin are discussed, namely X-ray fluorescence spectroscopy (XFS) and X-ray Raman scattering (XRS). Despite their fundamental differences, they require almost identical instrumentation and yield similar information. Both phenomena have a quasi-isotropic signal (4π sr) and, besides an intense X-ray source, they demand X-ray optics covering a large solid angle. The required energy resolution depends on the particular problem. The work described here has been performed with a ~1 eV multi-crystal analyzer, covering a total solid angle of up to 0.5% of 4π sr (Bergmann & Cramer, 1998). The experiments were carried out at beamline 10-2 at the Stanford Synchrotron Radiation Laboratory (SSRL) and beamline X-25 at the National Synchrotron Light Source (NSLS). The energy resolution of the incident beam was ~2 eV using Si (1,1,1) monochromators, and the flux was ~10^{11}–10^{12} photons s^{-1}.

2. X-ray fluorescence spectroscopy

The X-ray spectrum resulting from atomic fluorescence transitions has been a subject of study for more than a century. Substantial work has focused on identifying lines for elemental analysis and particle characterization, and to serve as detection channels for X-ray absorption spectroscopy (XAS) of dilute systems (Jaklevic *et al.*, 1977). Chemical effects on X-ray spectra have also been studied for a long time; an excellent overview can be found in a book by Meisel *et al.* (1989). Intense X-ray sources and efficient high-resolution analyzer devices now enable researchers to use XFS for quantitative physical, chemical and structural analysis, including the study of very dilute biological systems with weak fluorescence lines. Transition metals are of particular interest, because they occur in a variety of different chemical states and play an important role in catalytic processes.

Fig. 1 shows the total Mn *K* fluorescence spectrum for $Mn^{II}O$, in which the 1*s* electron is excited well above its binding energy. The spin-orbit split $K\alpha_1/K\alpha_2$ doublet ($2p \rightarrow 1s$; circles in Fig. 1) is at the lowest energy, while the eight-times-weaker $K\beta$ main region ($3p \rightarrow 1s$; squares in Fig. 1) is at 600 eV higher, split into $K\beta_{1,3}$ and $K\beta'$ through a 3*p*–3*d* exchange interaction. At even higher energies, much weaker transitions from valence levels are apparent after magnifying the spectrum by a factor of 500 (black solid line in Fig. 1). The $K\beta_{2,5}$ region results from a transition with ligand 2*p* as well as metal 4*p* and 3*d* character. The $K\beta''$ peak corresponds to ‘interatomic’ or ‘cross-over’ transitions from ligand valence levels. At excitation energies sufficient to create Mn 1*s* and 2*p* holes simultaneously, spectral features (grey line in Fig. 1) can be observed, even above the Fermi level indicated by the dashed line in Fig. 1. These lines, referred to as $KL\beta$ or $K\beta'''$, are $3p \rightarrow 1s$ transitions with a 2*p* spectator hole.

For Mn systems, pioneering work on $K\beta_{1,3}$ and $K\beta'$ lines was performed by Tsutsumi (1959), who used an X-ray tube for excitation and a film to record the spectra. Studies of the weaker spectral regions have been reported by, among others, Koster & Mendel (1970), Tsutsumi *et al.* (1976), Urch (1979), Mukoyama *et al.* (1986, 1990), Peng *et al.* (1994) and

very recently by Bergmann *et al.* (1999). $KL\beta$ lines have been extensively studied by, for example, Deutsch *et al.* (1996), and will not be discussed further in the following.

Using the example of a series of Mn oxides, it will now be discussed how different parts of the spectrum are affected by changes in the local Mn environment.

Fig. 2 shows the effects of the oxidation state of Mn on the different *K* emission features for $Mn^{II}O$ (solid lines), $Mn^{IV}O_2$ (dashed lines) and $KMn^{VII}O_4$ (circles). Both $K\alpha_1$ and $K\beta_{1,3}$ shift to lower energies with increasing oxidation state, whereas the $K\beta_{2,5}$ and $K\beta''$ peaks shift in the opposite direction. There are also changes in the shape and relative intensities of all features. The origin of the shifts of $K\alpha_1$ and $K\beta_{1,3}$ lies in the respective exchange interaction between the 2*p* and 3*p* hole with the unpaired 3*d* electrons. The Slater integrals for 2*p*–3*d* are smaller by a factor of 2 to 3 than those for 3*p*–3*d*. Consequently, $K\alpha_1$ shifts less than $K\beta_{1,3}$. The strongest shifts are observed for $K\beta_{2,5}$ and $K\beta''$ where, similar to the *K*-absorption edge, the shifts are to higher energy with higher oxidation state, reflecting an increase of the 1*s* binding energy when 3*d* electrons are removed. This difference indicates how $K\beta_{1,3}$ complements the *K* edge.

$K\beta_{1,3}$ XFS has been applied to characterize the oxidation states of the Mn cluster in photosystem II, the protein complex responsible for photosynthetic splitting of water and oxygen release (Bergmann *et al.*, 1998; Cinco *et al.*, 1998; Messinger *et al.*, 1998, 2000). In the catalytic Kok cycle, the Mn_4 cluster goes through a series of five *S* states (S_0–S_4), where a photon is absorbed at each of the first four steps and oxygen is released in the last one (Kok *et al.*, 1970). There is consensus that in each of the first two steps ($S_0 \rightarrow S_1$ and $S_1 \rightarrow S_2$) one of the four Mn atoms is oxidized (Yachandra *et al.*, 1996). Whether there is a Mn- or ligand-centered oxidation in the third step, $S_2 \rightarrow S_3$, is a disputed question (Ono *et al.*, 1992; Roelofs *et al.*, 1996; Iuzzolino *et al.*, 1998). Its answer has important consequences with regard to the mechanism of photosynthetic water splitting.

Fig. 3 shows the result of the first-moment analysis[†] of samples flashed through the Kok cycle, where zero flash (0F) corresponds to ~95% S_1, 1F to 80% S_2, 2F to 65% S_3, and 3F to 60% S_0, with the remaining populations in each sample in other *S* states. As seen in the left graph of Fig. 3, the shift between 1F (mostly S_2) and 2F (mostly S_3) is much smaller than in the other cases. For comparison, the inflection-point energies of XANES spectra from the same samples are shown (right side of Fig. 3), yielding a similar result. Both data sets independently suggest a ligand rather than direct Mn oxidation at $S_2 \rightarrow S_3$.

Another biocatalytic mechanism, which is not understood, is the Mn oxidation by bacteria. Manganese is an essential element for all living organisms. Transformations between soluble Mn^{II} and solid Mn^{IV} oxides catalyzed by bacteria are tightly coupled to changes in O_2 concentration. Because Mn oxide mineral surfaces are important sites for adsorption of inorganic and organic chemical species, these transformations can have a significant impact on the bio-availability of toxic wastes. Also, there is a scientific need to understand the

[†]The first moment is defined as $\langle E \rangle \equiv \Sigma(e_j i_j)/\Sigma(i_j)$ with e_j and i_j being the energy and intensity data points, respectively. An energy range from 6585 to 6595 eV was used.

processes and rates of manganese oxidation in order to interpret anomalous concentrations of manganese oxides in geological rock strata. Mn oxidation catalyzed by bacteria may have some unique mineralogical and chemical biosignatures, which could be used in studies of early life. It may lead to a different sequence of oxidation states, minerals and rates when compared to non-biological manganese oxidation under the same conditions of temperature, Mn^{II} concentration and time. There has been considerable discussion in the scientific literature over the question of whether the oxidation is a one-electron or two-electron process (Mandernack *et al.*, 1995; Nealson & Tebo, 1988; Tebo *et al.*, 1997). Fig. 4 shows preliminary results of $K\beta_{1,3}$ XFS on Bacillus SG-1 spores, isolated from Mn-coated sand grains from marine sediments (Rosson & Nealson, 1982).

The top spectrum in Fig. 4 shows the Mn $K\beta_{1,3}$ peak from minerals precipitated by SG-1 spores after spending 11.5 h in a 10 m*M* $Mn^{II}Cl_2$ solution (circles), compared with the best $Mn^{II}Mn^{IV}$ simulation, namely a mixture of 78% $Mn^{II}Cl_2$ and 22% birnessite (solid line). Birnessite is one of the known Mn^{IV}end products of the reaction. The $Mn^{II}Mn^{IV}$ spectrum is clearly too broad. Also allowing for Mn^{III} yields a much better result (bottom solid line in Fig. 4), where a mixture of 61.5% $Mn^{II}Cl_2$ and 38.5% $(Mn^{III})_2O_3$ gives the best fit. This result, which still has to be reproduced, indicates that despite its generally high reactivity, Mn^{III} seems to form as an intermediate in a one-electron two-step catalytic Mn oxidation by SG-1 spores.

As shown in Fig. 1, the spectral region above $K\beta_{1,3}$ contains several features, and in the following, the potential of using $K\beta''$ to gain detailed structural information is discussed. A recent study of $K\beta''$ 'interatomic' ligand (N, O, F) 2*s* to Mn 1*s* transitions (Bergmann *et al.*, 1999) showed that the energy of $K\beta''$ is very distinct for each ligand (shifting by ~5 eV, respectively) and the intensity of $K\beta''$ decreases exponentially with the ligand distance. It is estimated that the method can be used to determine distances to ~0.1 Å accuracy if the number of ligands is known. Besides transitions from F, O and N 2*s* levels, we have observed the 'interatomic' transition from the Cl 3*s* level, which has a binding energy very close to that of the N 2*s* level. Fig. 5 shows results for model compounds relevant to photosystem II.

Two sets of models, in which F is interchanged with Cl, are compared: set (*a*) tacnMn_2O_2**F**$_2$/**Cl**$_2$-tacn (Fig. 5*a*), and set (*b*) $[Mn_3O_4(\mathbf{F/Cl})(bpea)_3](ClO_4)_3$ (Fig. 5*b*). The vertical lines in Fig. 5 indicate the energy positions of expected $K\beta''$ peaks from different ligands. Spectra of compounds containing F and Cl are plotted with solid and dashed lines, respectively. The compounds in the top spectra have one F/Cl per Mn and a clear difference can be seen when comparing the F regions. In the bottom spectra this difference is still apparent but smaller, since only one F/Cl per three Mn atoms is present. Not surprisingly, the O peaks are strongest in all cases. In the top spectra, they result from two short O bonds at each of the di-μ-oxo bridged Mn atoms, and in the bottom spectra from di-μ-oxo and mono-μ-oxo bridges. The spectral region where a Cl feature is expected overlaps with that of the N ligands. The strength of the N peaks is weak, despite the large number of N ligands, since their distances are much longer. It appears that, in both Cl-containing systems, the signal in this region is somewhat stronger, which may be accounted for by a Cl peak. A more quantitative analysis, considering the exact ligand distances, is in progress.

These results demonstrate that with appropriate models and good data quality, $K\beta''$ features yield detailed structural information. Unlike EXAFS, $K\beta''$ XFS clearly discriminates between F, O and N, and it can be a useful tool for systems which defy structural analysis using other techniques. Because of the low intensity of $K\beta''$ (~10^{-4} of $K\alpha$), work on metalloproteins is difficult. We are currently trying to obtain $K\beta''$ spectra relevant to the binding of O and Cl to the Mn cluster of photosystem II. $K\beta''$ studies to determine the nature of the Fe–Ni bridging ligand in hydrogenase enzymes are also underway.

3. X-ray Raman scattering

X-ray absorption spectroscopy (XAS) at edges well below 1 keV encounters experimental difficulties, such as the need for ultra-high vacuum, small probe depth and related problems. Consequently, complex systems, liquids, reactive specimens, or samples under extreme conditions (temperature, pressure) often defy low-energy XAS analysis. Using hard X-rays as a probe avoids these difficulties; inelastic X-ray Raman scattering (XRS) is such a technique, having its largest cross section at low energy transfers (<500 eV).

The phenomenon was first noted in the early 20th century (Smekal, 1923; DuMond, 1933; Sommerfeld, 1936), but because of its weakness and the lack of an appropriate X-ray source, it took more than 20 years before first results were published. Starting with the work on polystyrene by Das Gupta (1959), several experimenters reported the observation of this effect, which was then sometimes called Smekal–Raman scattering (*e.g.* Das Gupta, 1962; Faessler & Mühle, 1966). However, to indicate how difficult the experiment was, others, including Weiss (1965), were not successful. Finally, the works by Mizuno & Ohmura (1967) and Suzuki (1967) started a series of papers based on experimental and theoretical results, which clearly established the close connection between XRS and XAS. Even until now this technique has not been widely used, and besides some demonstration experiments, there have been very few applications (Watanabe *et al.*, 1996; Bergmann *et al.*, 2000). The reason is mainly the extremely small cross section. From our measurements, we estimate that, for concentrated Li and C compounds, only ~10^{-8} of the incident photons contribute to the edge jump in a 1 eV energy slice integrated over 4π sr (this number includes the analyzer and detector efficiency). Even large-acceptance high-resolution analyzers collect only a small fraction of 4π sr (0.5% at our device). Nevertheless, a flux density of 10^{13}–10^{14} photons s^{-1} eV^{-1} (as provided by the most intense undulator beamlines) is sufficient to obtain a good spectrum in a matter of minutes in the most favorable cases, and X-ray Raman spectroscopy may become a routinely used tool in coming years. Besides its bulk sensitivity, X-ray Raman scattering, unlike conventional XAS, is not restricted by the dipole selection rule and has a q dependence, which can reveal the symmetry of unoccupied states (Schülke *et al.*, 1988; Krisch *et al.*, 1997).

Fig. 6 shows X-ray Raman results on the C edge of asphaltene, compared with coronene and paraffin, representing models of unsaturated and saturated carbon (Bergmann *et. al.*, 2000). Asphaltenes are complex mixtures of hetero-rich aromatic hydrocarbons that are present in solid suspension in crude oils. They dramatically affect the chemical and physical properties of crude oils, limiting the range of processes that can be utilized. Conventional C XANES

analysis on these materials suffers from saturation effects when using fluorescence detection and from surface oxidation when using photocurrent or electron yield detection.

The spectrum of paraffin (Fig. 6 top) shows a sharp edge with a shoulder at ~288 eV and the main $1s \rightarrow \sigma^*$ resonance at about 293 eV. By contrast, coronene (Fig. 6 middle) shows a $1s \rightarrow \pi^*$ resonance at about the same energy, as well as a feature at ~285 eV corresponding to a $1s \rightarrow \pi^*$ transition. The asphaltene (Fig. 6 bottom) exhibits a more diffuse edge spectrum, which is not surprising considering the complex mixture of molecules involved in this sample. Nevertheless, low-energy structure can be distinguished that clearly represents $1s \rightarrow \pi^*$ intensity, and a fit to the entire XANES region (282–320 eV) suggests a mixture of 50% aromatic and 50% saturated carbon. More qualitative analysis with a large set of models is in progress. Carbon is a prime candidate for XRS, and we are currently also studying Li compounds (batteries) and the oxygen *K* edge of aqueous systems.

4. Conclusions and outlook

The large increase in brightness provided by new synchrotron radiation facilities makes the rare interaction events of X-rays with matter attractive as a spectroscopic tool. Examples of X-ray fluorescence spectroscopy and X-ray Raman scattering have been discussed. There are countless potential applications of XRS as a bulk-sensitive hard X-ray probe to obtain XAS-type information for low-*Z* compounds. Both the X-ray sources and the X-ray optics are now available to perform such experiments on a routine basis and we are very optimistic with regard to the future development of this field of research.

Finally, a technique based on XFS, the so-called site-selective XAS, should also be mentioned. Here an XANES or EXAFS spectrum is recorded on a distinct feature of the X-ray fluorescence spectrum. If this feature is unique to a particular site in the system under study (*e.g.* its spin or oxidation state), the absorption spectrum will reflect the local structure or chemistry of this site. This additional discrimination can largely facilitate the XAS analysis of complex systems. We have obtained excellent $K\beta_{1,3}$-detected EXAFS spectra for $Fe_4[Fe(CN)_6]_3$ (prussian blue), in which the low-spin and high-spin sites could be separated (Glatzel *et. al.*, 2000). The obtained data quality indicates that such studies are also possible on very dilute systems.

Acknowledgments

This work was supported by the National Institutes of Health, grants GM-48145 (to SPC) and GM 55302 (to VKY), DOE grant DE-FG03-99ER62721 (to KHN) and by the Director, Office of Science, Office of Basic Energy Sciences and Office of Biological and Environmental Research, US Department of Energy, under contract DE-AC03-76SF00098. We thank our collaborators Professors K. Wieghardt, W. Armstrong and J.-J. Girerd, for providing the Mn model compounds. The National Synchrotron Light Source and the Stanford Synchrotron Radiation Laboratory are supported by the Department of Energy, Office of Basic Energy Sciences.

References

Bergmann U, Cramer SP. SPIE Proc. 1998; 3448:198–209.

Bergmann U, Grush MM, Horne CR, DeMarois P, PennerHahn JE, Yocum CF, Wright DW, Dube CE, Armstrong WH, Christou G, Eppley HJ, Cramer SP. J Phys Chem B. 1998; 102:8350–8352.

Bergmann U, Horne CR, Collins TJ, Workman JM, Cramer SP. Chem Phys Lett. 1999; 302:119–124.

Bergmann U, Mullins OC, Cramer SP. Anal Chem. 2000; 72:2609–2612. [PubMed: 10857643]

Cinco, RM.; Fernandez, C.; Messinger, J.; Robblee, JH.; Visser, H.; McFarlane, KL.; Bergmann, U.; Glatzel, P.; Cramer, SP.; Sauer, K.; Yachandra, VK.; Klein, MP. Photosynthesis: Mechanisms and Effects. Garab, G., editor. Dordrecht: Kluwer Academic Publishers; 1998. p. 1273-1278.

Das Gupta K. Phys Rev Lett. 1959; 3:38–40.

Das Gupta K. Phys Rev. 1962; 128:2181–2188.

Deutsch M, Gang O, Hämäläinen K, Kao CC. Phys Rev Lett. 1996; 76:2424–2427. [PubMed: 10060696]

DuMond JW. Rev Mod Phys. 1933; 5:1–33.

Faessler A, Mühle P. Phys Rev Lett. 1966; 17:4–5.

Glatzel P, Jacquamet L, Bergmann U, de Groot FMF, Cramer SP. Angew Chem. 2000 Submitted.

Iuzzolino L, Dittmer J, Doerner W, Meyer-Klaucke W, Dau H. Biochemistry. 1998; 37:17112–17119. [PubMed: 9860823]

Jaklevic J, Kirby JA, Klein MP, Robertson AS, Brown GS, Eisenbeger P. Solid State Commun. 1977; 23:679–682.

Kok B, Forbush B, McGloin M. Photochem Photobiol. 1970; 11:457–475. [PubMed: 5456273]

Koster AS, Mendel H. Phys Chem Solids. 1970; 31:2511–2522.

Krisch MH, Sette F, Masciovecchio C, Verbeni R. Phys Rev Lett. 1997; 78:2843–2846.

Mandernack KW, Post J, Tebo BM. Geoch Cosmoch Acta. 1995; 59:4393–4408.

Meisel, A.; Leonhardt, G.; Szargan, R. X-ray Spectra and Chemical Binding. In: Kallne, E.; Deslattes, RD., translators and editors. Springer Series in Chemical Physics. Vol. 37. Berlin: Springer-Verlag; 1989.

Messinger, J.; Robblee, JH.; Fernandez, C.; Cinco, RM.; Visser, H.; Bergmann, U.; Glatzel, P.; Cramer, SP.; Campbell, KA.; Peloquin, JM.; Britt, RD.; Sauer, K.; Yachandra, VK.; Klein, MP. Photosynthesis: Mechanisms and Effects. Garab, G., editor. Dordrecht: Kluwer Academic Publishers; 1998. p. 1279-1282.

Messinger J, Robblee JH, Bergmann U, Fernandez C, Glatzel P, Visser H, Cinco RM, McFarlane KL, Belacchio E, Pizarro SA, Cramer SP, Sauer K, Yachandra VK. J Am Chem Soc. 2000 Submitted.

Mizuno Y, Ohmura Y. J Phys Soc Jpn. 1967; 22:445–449.

Mukoyama K, Taniguchi K, Adachi H. Phys Rev B. 1986; 34:3710.

Mukoyama T, Taniguchi K, Adachi H. Phys Rev B. 1990; 41:8118–8121.

Nealson KH, Tebo BM. Adv Appl Microbiol. 1988; 33:279–318.

Ono T, Noguchi T, Inoue Y, Kusunoki M, Matsushita T, Oyanagi H. Science. 1992; 258:1335–1337. [PubMed: 17778358]

Peng G, Degroot FMF, Hämäläinen K, Moore JA, Wang X, Grush MM, Hastings JB, Siddons DP, Armstrong WH, Mullins OC, Cramer SP. J Am Chem Soc. 1994; 116:2914–2920.

Roelofs TA, Liang W, Latimer MJ, Cinco RM, Rompel A, Andrews JC, Sauer K, Yachandra VK, Klein M. Proc Natl Acad Sci USA. 1996; 93:3335–3340. [PubMed: 11607649]

Rosson RA, Nealson KH. J Bacteriol. 1982; 151:1027–1034. [PubMed: 6212577]

Schülke W, Bonse U, Nagasawa H, Kaprolat A, Berthold A. Phys Rev B. 1988; 38:2112–2123.

Smekal A. Naturwissenschaften. 1923; 11:873–875.

Sommerfeld A. Phys Rev. 1936; 50:38–40.

Suzuki T. J Phys Soc Jpn. 1967; 22:1139–1149.

Tebo, BM.; Ghiorse, WC.; van Waasbergen, LG.; Siering, PL.; Caspi, R. Geomicrobiology: Interactions Between Microbes and Minerals, Reviews in Microbiology. Banfield, JF.; Nealson, KH., editors. Vol. 35. Washington, DC: Mineralogical Society of America; 1997. ch. 7

Tsutsumi K. J Phys Soc Jpn. 1959; 14:1696–1706.

Tsutsumi K, Nakamori H, Ichikawa K. Phys Rev B. 1976; 13:929–933.

Urch, DS. X-ray Emission Spectroscopy. Urch, DS., editor. Vol. 3. New York: Academic Press; 1979. p. 1-39.

Watanabe N, Hayashi H, Udagawa Y, Takeshita K, Kawata H. Appl Phys Lett. 1996; 69:1370–1372.

Weiss RJ. Phys Rev. 1965; 140:A1867–A1868.
Yachandra VK, Sauer K, Klein MP. Chem Rev. 1996; 96:2927–2950. [PubMed: 11848846]

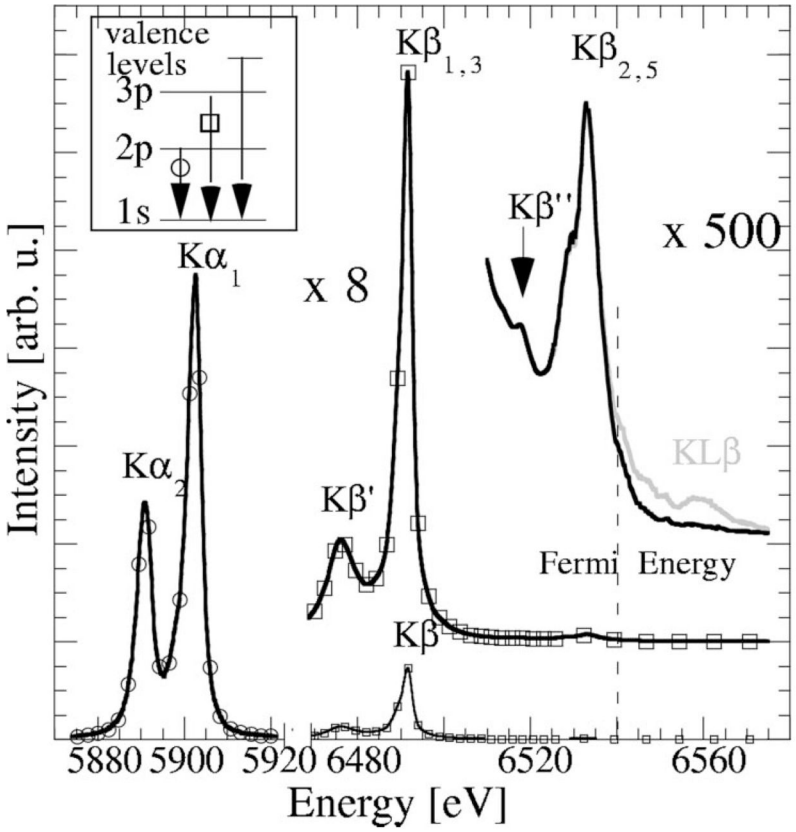

Figure 1.
Mn *K* fluorescence spectrum of $Mn^{II}O$. Inset: schematic transition scheme.

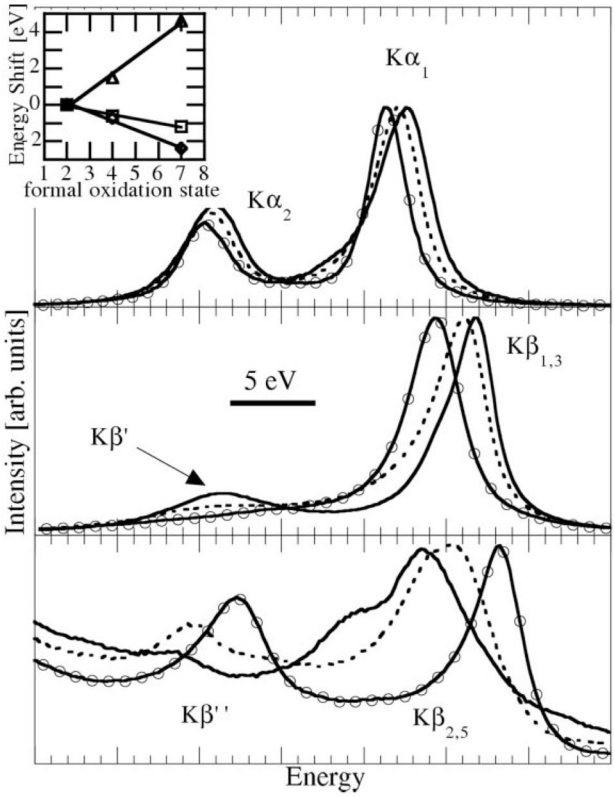

Figure 2.

K fluorescence features for $Mn^{II}O$ (solid lines), $Mn^{IV}O_2$ (dashed lines) and $KMn^{VII}O_4$ (circles) and corresponding shifts of $K\alpha_1$ (squares), $K\beta_{1,3}$ (diamond) and $K\beta_{2,5}$ (triangles).

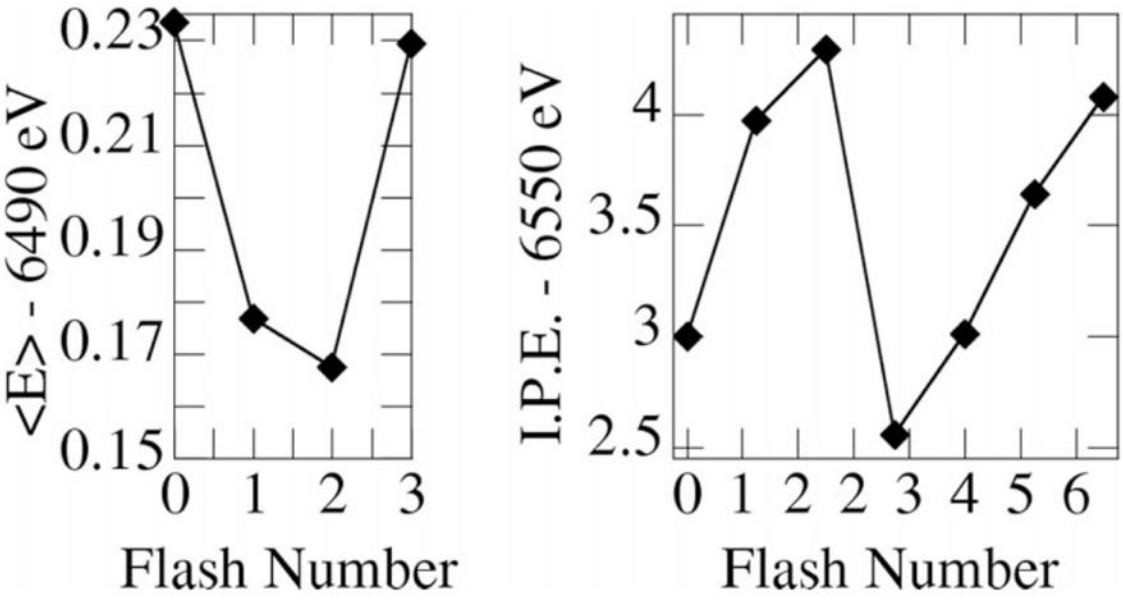

Figure 3.

First moment of the Mn $K\beta_{1,3}$ peak (left) and the XANES inflection-point energy (right) of photosystem II as a function of flash number. The S_1 state corresponds to zero flashes.

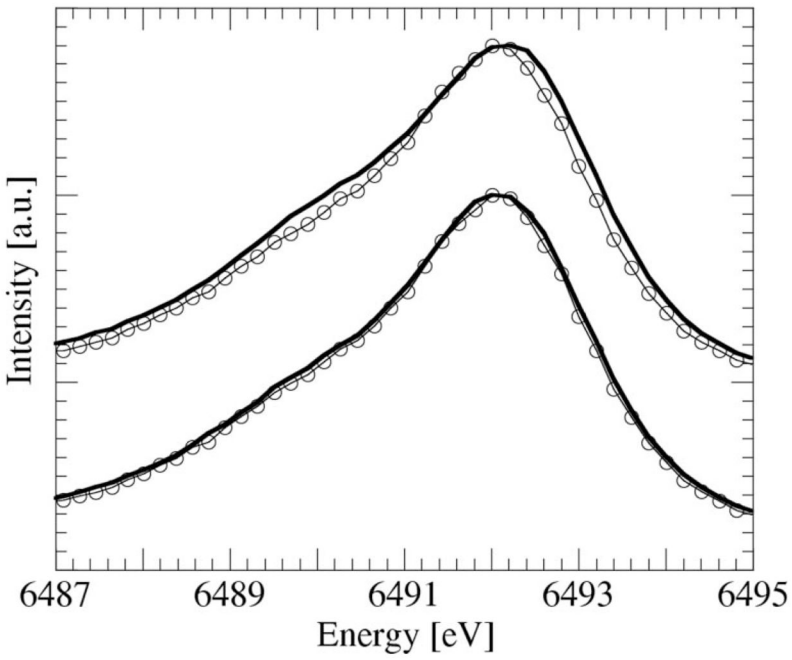

Figure 4.

$K\beta_{1,3}$ spectrum of crystallites from SG-1 spores after 11.5 h in 10 m*M* $Mn^{II}Cl_2$ solution (circles). Top: best fit using only Mn^{II} and Mn^{IV}. Bottom: best fit allowing for Mn^{II}, Mn^{III} and Mn^{IV}.

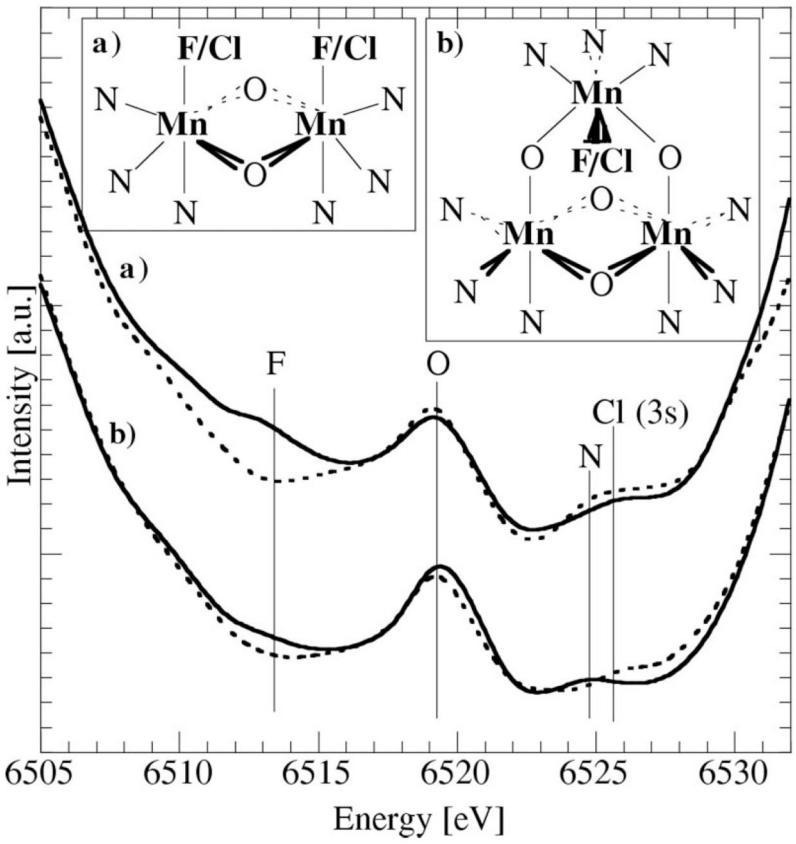

Figure 5.

$K\beta''$ region of two sets of models, where F (solid lines) is interchanged with Cl (dashed lines). Top insets: local Mn structure for each set.

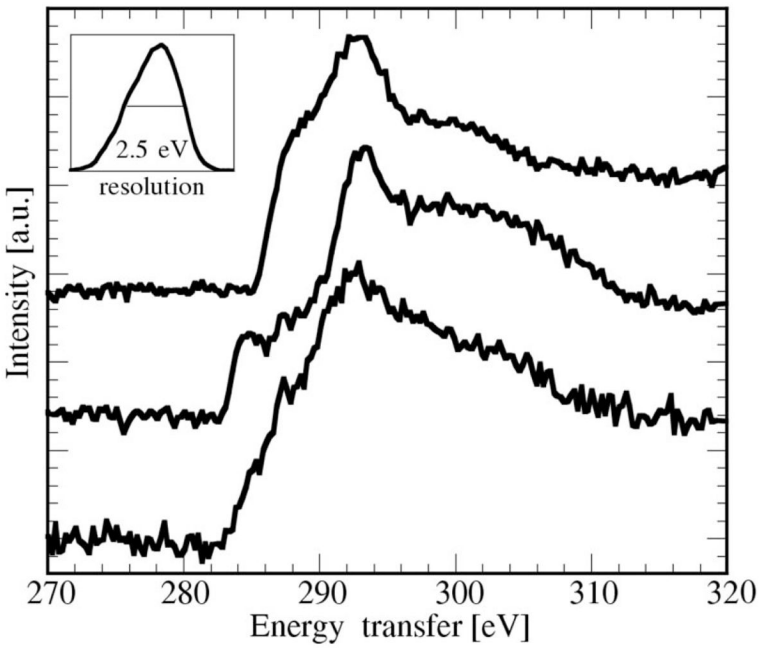

Figure 6.

X-ray Raman spectra of (top to bottom): paraffin, coronene and asphaltene. Inset: measured energy resolution of the elastic peak, resulting from convolution of the incident-beam resolution and the analyzer resolution.